SWAMSI: Bistatic CSAS and Target Echo Studies

Kent Scarbrough
Advanced Technology Laboratory
Applied Research Laboratories
The University of Texas at Austin
P.O. Box 8029
Austin, TX 78713-8029
phone: (512) 835-3364 email: kscarbrough@arlut.utexas.edu

Stephen K. Mitchell
Advanced Technology Laboratory
Applied Research Laboratories
The University of Texas at Austin
P.O. Box 8029
Austin, TX 78713-8029
phone: (512) 835-3686 email: mitchell@arlut.utexas.edu

Award Number: N00014-06-G-0218; Delivery Order 0004

LONG TERM GOALS

Develop Circular Synthetic Aperture Sonar (CSAS) techniques and signal processing algorithms to generate high resolution acoustic images of mine and non-mine targets using bistatic and multistatic sonar configurations.

OBJECTIVES

The objective of this work is to demonstrate the feasibility of Autonomous Underwater Vehicle (AUV) based bistatic CSAS imaging of bottom mines and mine-like targets, to evaluate and compare the quality of bistatic imaging relative to monostatic imaging, and to determine the practical advantages (or disadvantages) of bistatic imaging with respect to monostatic imaging.

APPROACH

Most synthetic aperture sonar (and radar) systems operate in a monostatic mode in which the source and receiver are collocated. To generate a monostatic CSAS image, the target region is partially or completely circled by the sonar and echoes are acquired over a large range of target aspects. Detailed images of target outlines can be produced from this data even at relatively low transmit frequencies (tens of kHz) [1,3]. In the bistatic mode, the source and receiver are separated in space and the geometry considerations are somewhat more complicated [2,3].

Under this task, bistatic CSAS imaging algorithms have been developed as extensions to the monostatic CSAS imaging algorithms previously developed at ARL:UT. Bistatic CSAS image processing is based upon Fourier Transform reconstruction techniques similar to those in [4-6] with significant modifications to accommodate the bistatic configuration [1,3].

Report Documentation Page

Form Approved
OMB No. 0704-0188

1. REPORT DATE	2. REPORT TYPE	3. DATES COVERED
30 SEP 2007	**Annual**	**00-00-2007 to 00-00-2007**

4. TITLE AND SUBTITLE	5a. CONTRACT NUMBER
SWAMSI: Bistatic CSAS And Target Echo Studies	5b. GRANT NUMBER
	5c. PROGRAM ELEMENT NUMBER
6. AUTHOR(S)	5d. PROJECT NUMBER
	5e. TASK NUMBER
	5f. WORK UNIT NUMBER
7. PERFORMING ORGANIZATION NAME(S) AND ADDRESS(ES) **The University of Texas at Austin,Applied Research Laboratories,Advanced Technology Laboratory, P.O. Box 8029,Austin,TX,78713**	8. PERFORMING ORGANIZATION REPORT NUMBER
9. SPONSORING/MONITORING AGENCY NAME(S) AND ADDRESS(ES)	10. SPONSOR/MONITOR'S ACRONYM(S)
	11. SPONSOR/MONITOR'S REPORT NUMBER(S)

12. DISTRIBUTION/AVAILABILITY STATEMENT
Approved for public release; distribution unlimited

13. SUPPLEMENTARY NOTES
code 1 only

14. ABSTRACT
The objective of this work is to demonstrate the feasibility of Autonomous Underwater Vehicle (AUV) based bistatic CSAS imaging of bottom mines and mine-like targets, to evaluate and compare the quality of bistatic imaging relative to monostatic imaging, and to determine the practical advantages (or disadvantages) of bistatic imaging with respect to monostatic imaging.

15. SUBJECT TERMS

16. SECURITY CLASSIFICATION OF:			17. LIMITATION OF ABSTRACT	18. NUMBER OF PAGES	19a. NAME OF RESPONSIBLE PERSON
a. REPORT	b. ABSTRACT	c. THIS PAGE			
unclassified	**unclassified**	**unclassified**	**Same as Report (SAR)**	**9**	

Initial evaluation of bistatic CSAS imaging was performed using data acquired from the "rotating seabed" at ARL:UT's Lake Travis Test Station (LTTS). Recent efforts have focused on demonstrating the feasibility of bistatic CSAS imaging using data acquired from a mobile platform at LTTS as well as using available sea test data from other projects. Future efforts will focus on data acquired in conjunction with the ARTEMIS Autonomous Underwater Vehicle (AUV). Tests are planned to be conducted both at Lake Travis and at-sea.

WORK COMPLETED

Previous reporting demonstrated the feasibility of bistatic CSAS using target data acquired under laboratory conditions with the Rotating Seabed, a 6 m diameter, sand-filled turntable at LTTS. This report presents CSAS imaging results in the 40-70 kHz band for the same targets on the Lake Travis lake bottom and work in progress towards bistatic imaging with an AUV in the 50-100 kHz band.

The Rotating Seabed is suspended below the LTTS barges at a depth of ~9 m. For the monostatic configuration, the target is positioned at the center of the turntable and is rotated while the co-located source and receiver remain fixed. To achieve a bistatic configuration, the target is positioned near one edge of the platter while a projector is mounted near the opposite edge of the platter. Both target and projector are rotated with the platter, and the receiver remains fixed. This allows bistatic data to be acquired with the source at a fixed orientation relative to the target and with the receiver at varying aspects with respect to the source and target as the platter is rotated.

To acquire data for bottom targets from a mobile receiver at LTTS, a sonar source and receiver were mounted on a column on a mobile barge. Data were acquired while the barge moved in a circle around a target field on a relatively flat portion of the lake bottom near Mansfield Dam at Lake Travis. The target depths were approximately 10 m, and the diameter of the sonar path was approximately 120 m. For monostatic data, a beacon placed near the center of the target field is used as a micro-positioning aid. For bistatic data, the column-mounted source is not used; the beacon serves both to ensonify the target field and for micro-positioning.

Under the DARPA-sponsored ARTEMIS project, ARL:UT acquired a Bluefin-12 AUV in October 2006. Integration of the sonar payload section and initial testing of the AUV and sonar payload was completed at Lake Travis in December 2006, see Fig. 1. The sonar payload, designed and fabricated at ARL:UT, operates in the 55-95 kHz range. The frequency band was selected as low as practical, consistent with providing quality images and AUV size constraints, to relax the SAS navigation requirements as much as possible. The curved projector, seen on top of the black sonar payload section in Fig. 1, has a 90° horizontal beamwidth and a 15° vertical beamwidth. The projector has a 5° downward pre-steering angle; eight independently driven rows of elements allow electronic vertical beam-steering. The receive array, on the side of the sonar payload, not visible in Fig. 1, consists of 48 elements, 4 high x 12 wide. The nominal horizontal beamwidth is 5°, while the vertical beamwidth is 15°. The receive array may be mechanically pre-steered from -10° to 0° in the vertical. When surfaced, timing is synchronized using a GPS pulse-per-second (PPS) timing pulse. When submerged, an oven-controlled crystal oscillator provides the required, highly stable, system reference frequency.

A buoy-based, synchronized beacon, shown in Fig. 1, was developed for use with the ARTEMIS AUV for both monostatic and bistatic CSAS imaging trials. For the current proof-of-concept system, the beacon is hand-deployed at the nominal center of the area to be imaged. For the monostatic case, the beacon serves as a micro-navigation aid; for the bistatic case, the beacon is used as the source as well as for micro-navigation. The AUV circles the target area at a radius of 50-100 m. At a speed of 1 m/s, a circle track is completed in approximately 5-10 minutes, depending on the radius. The inner circular region corresponding to half the radius of the AUV path is imaged. The projector's 90° horizontal beamwidth will ensonify the inner half-radius circle even with ±15° sway about the intended track.

The ARTEMIS AUV participated in AUVFest 2007 and work is on-going to acquire and analyze additional monostatic and bistatic data to evaluate AUV-based CSAS imaging.

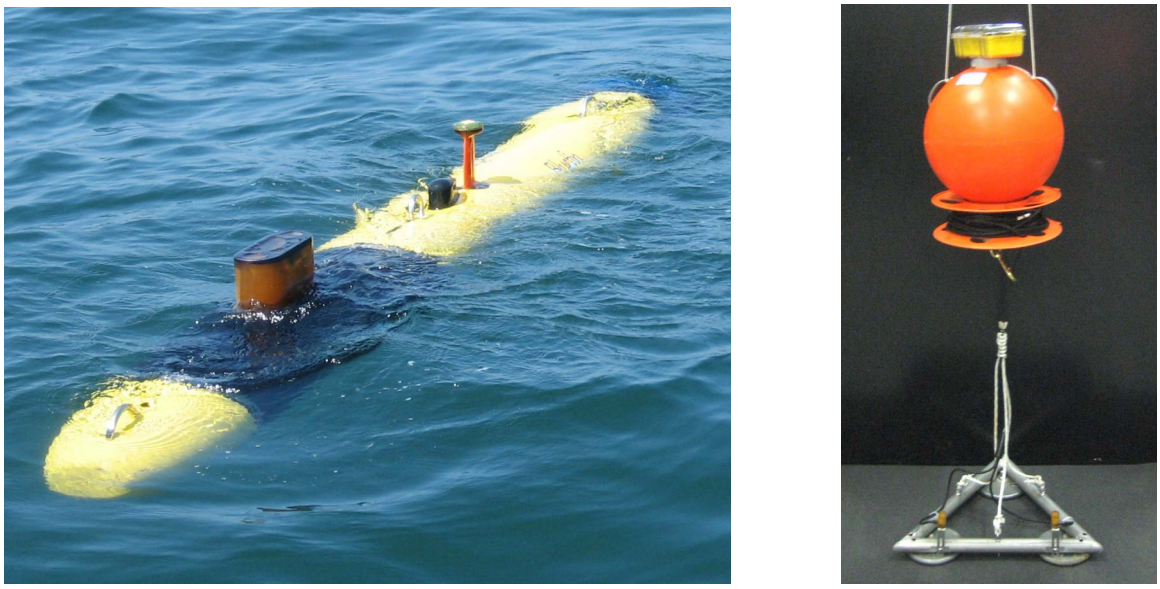

Figure 1. ARTEMIS Bluefin-12 AUV with CSAS Payload (left) and Buoy-Based Synchronized Beacon System (right)

In addition, work is beginning to acquire target data in the frequency band of 2-20 kHz, using a parametric source acquired under a DURIP grant. ARL:UT contracted with NUWCDIVNPT for the fabrication of a custom-built, 15 inch diameter, piezocomposite transducer capable of parametric mode operation, shown in Fig. 2. The electrode patterns are also shown in Fig. 2. Selecting different combinations of electrodes allows selection of the following transmit apertures (and thereby control of transmit beamwidth):

1. Aperture A: circular – 15 inch diameter,

2. Aperture B: circular – 8 inch diameter, and

3. Aperture C: "rectangular" Strip – 4 inches x 15 inches.

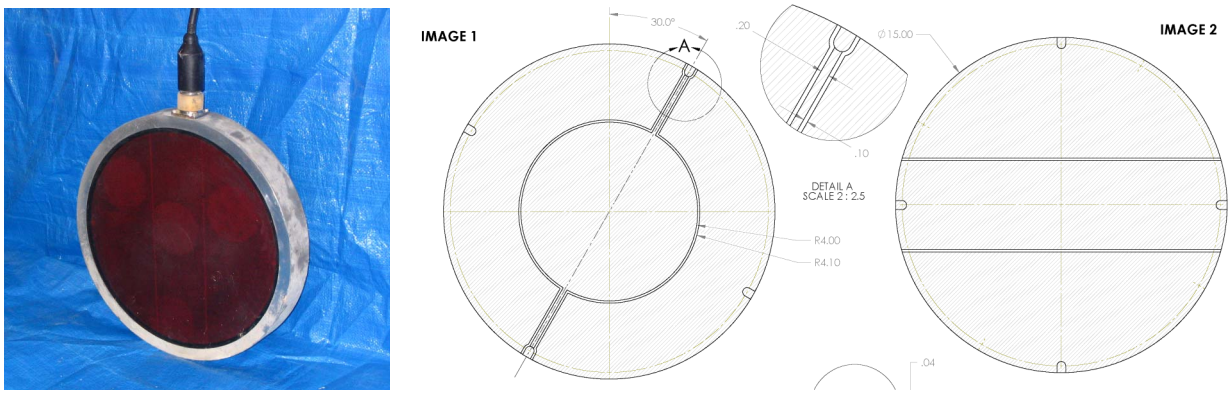

Figure 2. Parametric projector (left) and Front/Back Electrode Patterns (right).

RESULTS

The images shown in Fig. 3, generated from LTTS turntable data, have been reported previously, but are included here for reference. Fig. 3 compares monostatic and bistatic images from a steel cylinder. In Fig. 3B, the portions of the target ensonified by the bistatic fixed source are imaged very well. At the bottom of Figure 3B, the cylinder is observed to shadow the turntable edge.

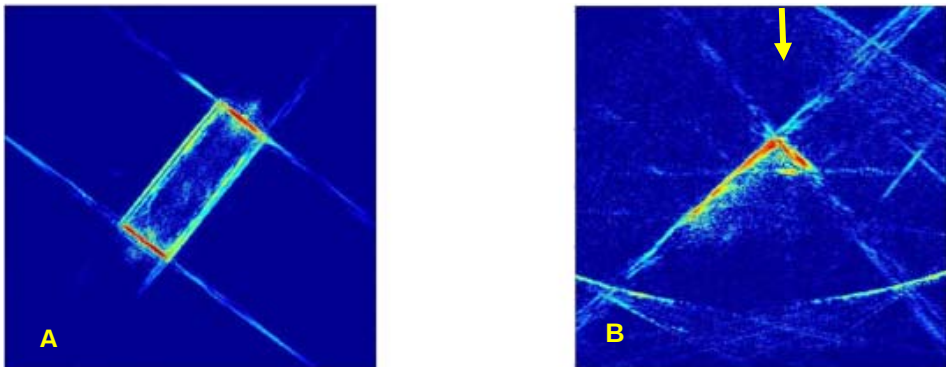

A. Monostatic ***B. Bistatic***

Figure 3. CSAS Images of steel cylinder. A. Monostatic image. B. Bistatic image of cylinder near edge of turntable; yellow arrow indicates source direction.

The signal processing used to generate CSAS images is similar to Fourier image reconstruction technique used for circular synthetic aperture radar [4]. The first step is to compute the spectrum of the echo data to obtain data in the frequency vs. angle domain, refer to [1,2] for a more detailed description. This is followed by a polar-to-rectangular transformation to obtain the wavenumber space representation, $\boldsymbol{M(k_x,k_y)}$. Figure 4 compares the monostatic and bistatic wavenumber space representations corresponding to the monostatic and bistatic images of the steel cylinder shown in Figure 3. While the monostatic and bistatic wavenumber data are significantly different, both contain the information needed to reconstruct the cylinder image.

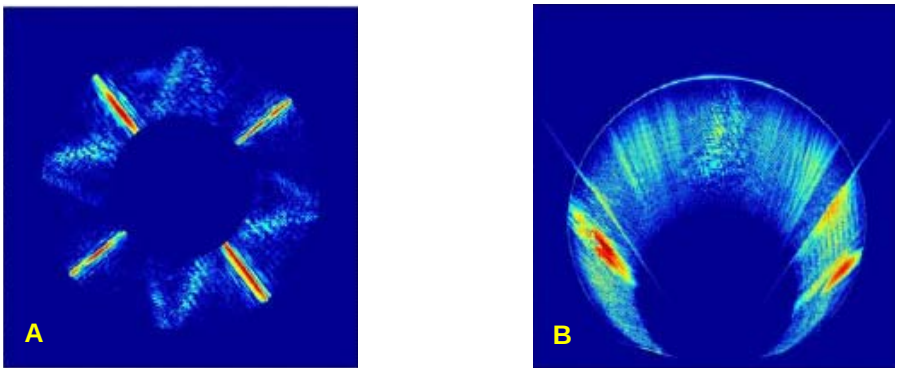

A. Monostatic ***B. Bistatic***

Figure 4. Monostatic and bistatic steel cylinder wavenumber data amplitudes. A. Monostatic scale: ± 1000 m^{-1} for k_x, k_y. B. Bistatic scale: ± 500 m^{-1} k_x, 0-1000 m^{-1} k_y.

The first test of monostatic and bistatic CSAS imaging from a moving platform was conducted at Lake Travis using the mobile barge. A receive array and projector were mounted on a column on the mobile barge and an early prototype of a two-pinger beacon was positioned near the center of a target field. Several mine shapes and other bottom objects were positioned on a relatively flat portion of lake bottom near Mansfield Dam at Lake Travis. Data were acquired while the barge moved in a circular path around the target field Target depths were approximately 12 m, the sonar depth on the mobile barge was ~3 m, and the diameter of the sonar path was approximately 120 m. For bistatic data, the column-mounted source was not used; the beacon served both to ensonify the target field and for micro-positioning.

The bistatic sinogram, the time aligned waterfall of matched filter echo data, is shown on the left of Fig. 5 for 30 ms of received data for 2000 pings, which correspond to slightly more than one full circle around the target field by the receiver. The TVG values, applied to compensate for the decrease in received level as a function of range, are displayed at ranges of 1, 10, and 20 m along the bottom of this figure. Comparing the bistatic sinogram in Figure 5 with the corresponding monostatic sonogram [2], two major differences are observed. As expected, the bistatic sinogram “loops” or target tracks are only seen for a half cycle not a full cycle as the targets are ensonified over only 180° of aspect by the fixed source. In addition, the reverberation level is generally much lower for the bistatic data; the only significant energy in the sinogram are echoes from targets and rocks. The low reverberation is likely attributable to the shallow grazing angle, ~2° or less, between the source and the bottom in the target region for the bistatic case, compared to an angle of nearly 10° for the monostatic case.

After computing the aligned bistatic sinogram, the focus times for the center points of 49 tiles that covered the 28 m x 28 m target region were calculated. For each tile, a refocused sinogram (with a 3° receiver beamwidth) was computed and the bistatic image processing algorithm was implemented. The bistatic wavenumber data amplitudes for each of the 49 tiles are shown on the right side of Fig. 5. Note that the source direction is different for each tile and the crescent wavenumber representation shapes orient towards the source.

Figure 6 compares monostatic and bistatic CSAS images of the full target field. The monostatic image may be used as a reference for the performance of the bistatic configuration. For the monostatic image,

all parts are insonified from all directions. The monostatic image clearly shows bottom texture and bottom features, scattered rocks, plus several well-defined target objects. Looking at the bistatic image, a first impression is the lack of definition of the bottom texture; the general image is much darker. This is reasonable if one considers that the monostatic insonification is from a grazing angle is approximately 10°, but the bistatic insonification (source just above the bottom) is less than 1°. Looking at target objects, one can see that the parts of deployed targets and scattered rocks that are ensonified by the fixed source at the center of the field are seen in the bistatic image. Several of these objects are compared in more detail in Figs. 7-9. The one complete object that can be recognized in both the monostatic and bistatic images is the rectangular lobster trap located right center in each image.

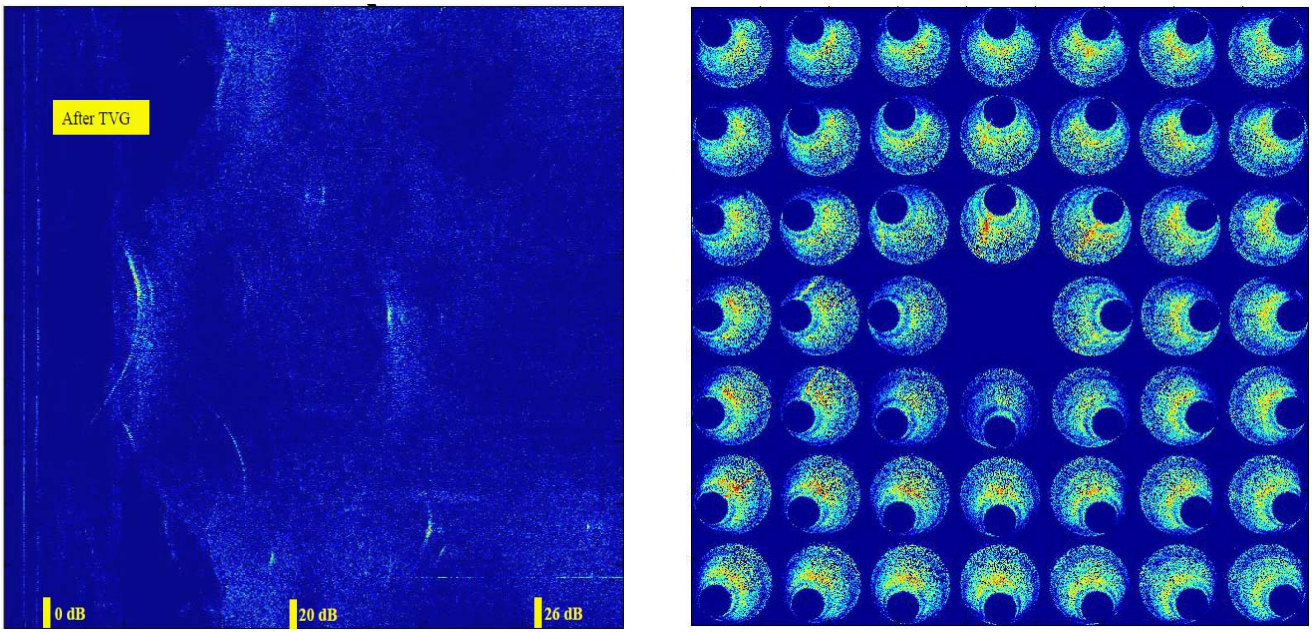

Figure 5. Left: Bistatic Sinogram. 2000 pings, 30 ms. Data aligned to direct arrival of beacon signal. TVG values at 1, 10, and 20 m ranges shown at bottom. Right: Bistatic wavenumber data for 49 tiles covering target region, centered on source. Each tile is spatially located in the horizontal plane; the content of each tile has dimensions of m^{-1}.

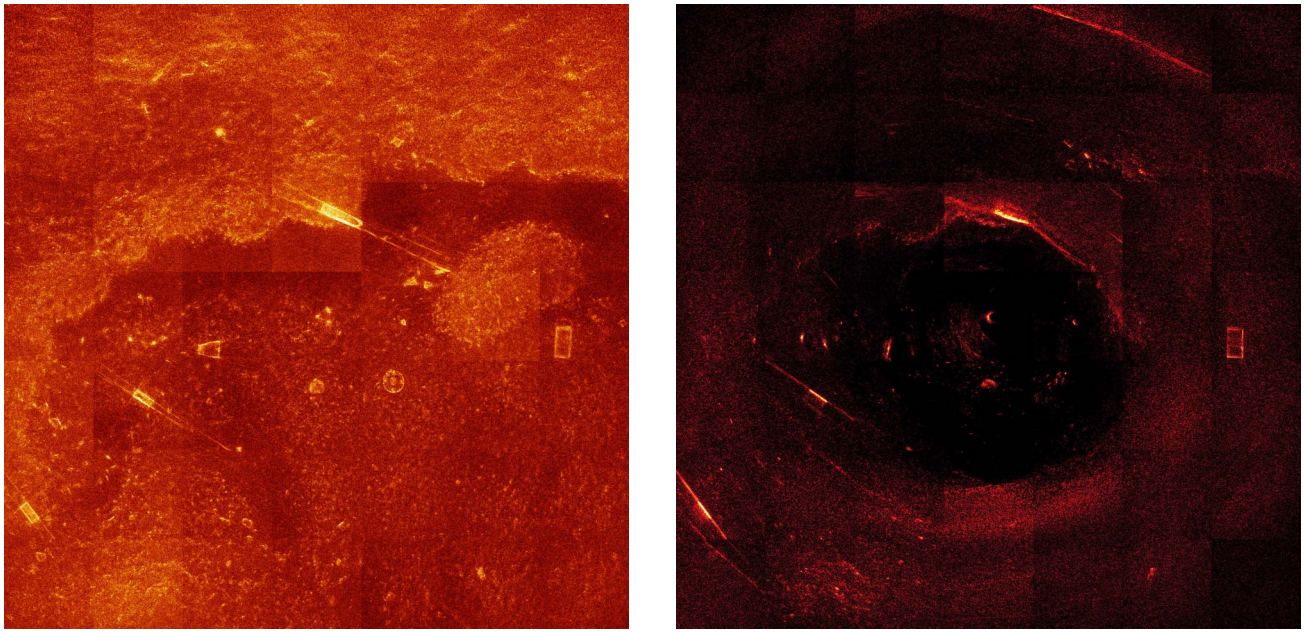

a. Monostatic ***b. Bistatic***

Figure 6. CSAS Images of 29m x29m Region. In the bistatic case, the source is at the center of the field; only the target facets facing the center (the source) are insonified and imaged.

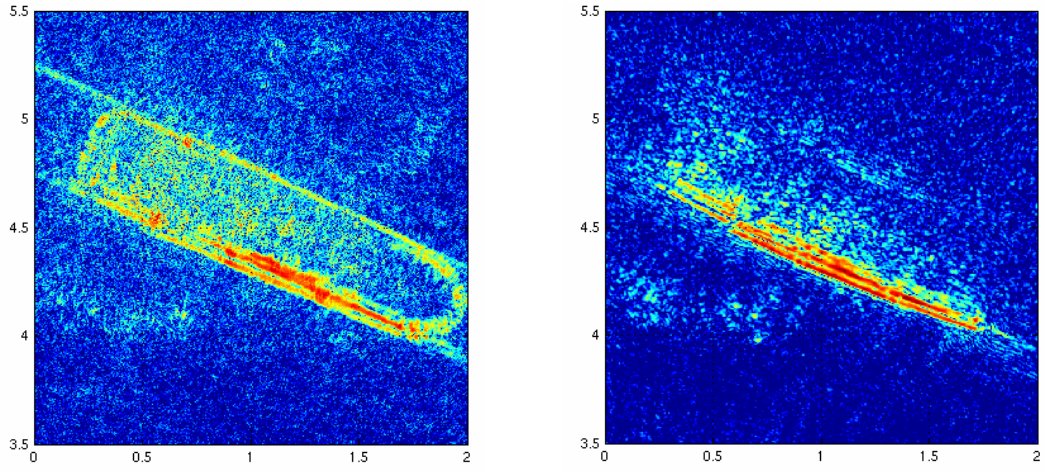

a. Monostatic ***b. Bistatic***

Figure 7. Monostatic and bistatic images of cylindrical mine shape located top center in Fig. 3.

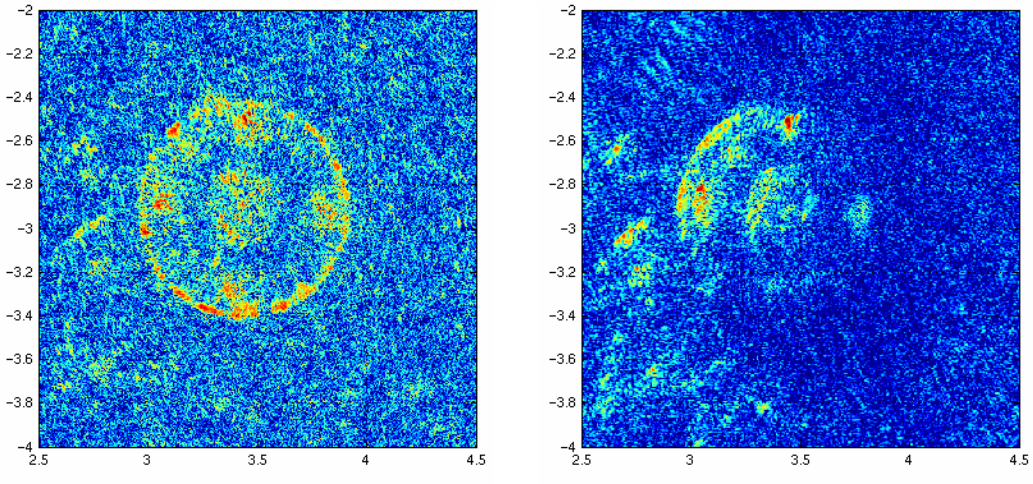

a. Monostatic ***b. Bistatic***

Figure 8. Monostatic and bistatic images of conical mine shape right of center in Fig. 3.

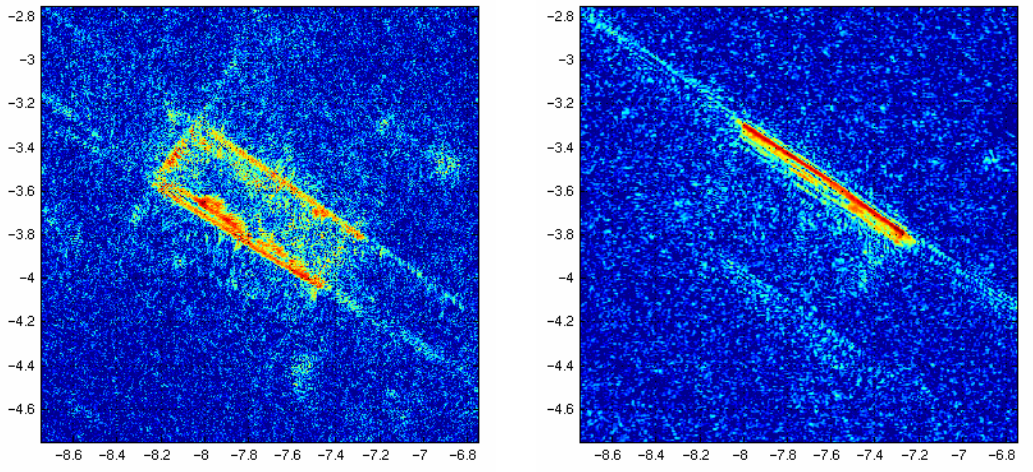

a. Monostatic ***b. Bistatic***

Figure 9. Monostatic and bistatic images of steel cylinder left of center in Fig. 3.

IMPACT/APPLICATIONS

The results of this work will lead to the development of improved AUV-based imaging methods for bottom mine and non-mine classification and identification.

RELATED PROJECTS

Efforts under this project are being coordinated with the other projects funded under the ONR Shallow Water Autonomous Mine Sensing Initiative (SWAMSI) program and with the DARPA-funded ARTEMIS project.

PUBLICATIONS

"Bistatic SAS imaging studies," SK Mitchell, KN Scarbrough, SP Pitt, Proceedings of the Institute of Acoustics, London, Vol. 28. Pt.5. 2006. (Presented to the International Conference on Synthetic Aperture Sonar and Synthetic Aperture Radar, Lerici, Italy, 11-12 September, 2006.)

REFERENCES

[1] S.K. Mitchell, K.N. Scarbrough, S.P. Pitt, T.L. Kooij, "High Resolution Circular SAS with Controlled Focus," Proceedings of the Institute of Acoustics, London, Vol. 28. Pt.5. 2006. (Presented to the International Conference on Synthetic Aperture Sonar and Synthetic Aperture Radar, Lerici, Italy, 11-12 September, 2006.)

[2] S.K. Mitchell, K.N. Scarbrough, SP Pitt, "Bistatic SAS imaging studies," Proceedings of the Institute of Acoustics, London, Vol. 28. Pt.5. 2006. (Presented to the International Conference on Synthetic Aperture Sonar and Synthetic Aperture Radar, Lerici, Italy, 11-12 September, 2006.)

[3] S.K. Mitchell, "High Resolution Bistatic and Monostatic Circular SAS Imaging at Search Frequencies, " Proc. of Sixth Int'l Symp. on Technology and the Mine Problem, Monterey, California, 9-13 May 2004.

[4] D.C. Munson, Jr., J. D. O'Brien, W.K. Jenkins, "A Tomographic formulation of spotlight-mode synthetic aperture radar, " Proc. IEEE, vol. 71, pp. 917-325, Aug. 1983.

[5] A.C. Kac and M. Slaney, Principles of Computerized Tomographic Imaging, IEEE Press, New York, NY, 1988.

[6] Yong Wu and David C. Munson, Jr., "Synthetic Aperture Imaging of Aircraft using Reflected Television Signals, " Proc. of SPIE, Algorithms for synthetic aperture radar imagery VIII, vol. 4382, Orlando, FL, Apr. 16-19 2001.